Title
Measurements of Hydroxyl Radical Concentrations during Indoor Cooking Events: Evidence of an Unmeasured Photolytic Source of Radicals

Journal
Environmental Science and Technology, 57(2)

ISSN
0013-936X

Authors
Reidy, Emily
Bottorff, Brandon P
Rosales, Colleen Marciel F
et al.

Publication Date
2023-01-17

DOI
10.1021/acs.est.2c05756

Peer reviewed

Environmental Science & Technology

pubs.acs.org/est

Article

Measurements of Hydroxyl Radical Concentrations during Indoor Cooking Events: Evidence of an Unmeasured Photolytic Source of Radicals

Emily Reidy,* Brandon P. Bottorff, Colleen Marciel F. Rosales, Felipe J. Cardoso-Saldaña, Caleb Arata, Shan Zhou, Chen Wang, Andrew Abeleira, Lea Hildebrandt Ruiz, Allen H. Goldstein, Atila Novoselac, Tara F. Kahan, Jonathan P. D. Abbatt, Marina E. Vance, Delphine K. Farmer, and Philip S. Stevens*

Cite This: *Environ. Sci. Technol.* 2023, 57, 896−908

Read Online

ACCESS | Metrics & More | Article Recommendations | Supporting Information

ABSTRACT: The hydroxyl radical (OH) is the dominant oxidant in the outdoor environment, controlling the lifetimes of volatile organic compounds (VOCs) and contributing to the growth of secondary organic aerosols. Despite its importance outdoors, there have been relatively few measurements of the OH radical in indoor environments. During the House Observations of Microbial and Environmental Chemistry (HOMEChem) campaign, elevated concentrations of OH were observed near a window during cooking events, in addition to elevated mixing ratios of nitrous acid (HONO), VOCs, and nitrogen oxides (NO_X). Particularly high concentrations were measured during the preparation of a traditional American Thanksgiving dinner, which required the use of a gas stove and oven almost continually for 6 h. A zero-dimensional chemical model underpredicted the measured OH concentrations even during periods when direct sunlight illuminated the area near the window, which increases the rate of OH production by photolysis of HONO. Interferences with measurements of nitrogen dioxide (NO_2) and ozone (O_3) suggest that unmeasured photolytic VOCs were emitted during cooking events. The addition of a VOC that photolyzes to produce peroxy radicals (RO_2), similar to pyruvic acid, into the model results in better agreement with the OH measurements. These results highlight our incomplete understanding of the nature of oxidation in indoor environments.

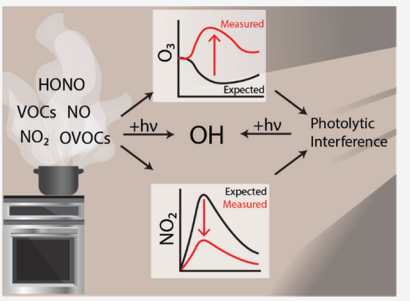

KEYWORDS: *hydroxyl radical (OH), indoor oxidants, photochemistry*

1. INTRODUCTION

The hydroxyl radical (OH) is the dominant outdoor oxidant, but its potential importance indoors has only recently been investigated. OH radical production outdoors occurs primarily through ultraviolet (UV) photolysis of ozone (O_3), nitrous acid (HONO), formaldehyde, and other oxygenated volatile organic compounds (VOCs) and has been extensively studied.[1−11] While solar UV light is strongly filtered by windows, a significant fraction of wavelengths between 320−400 nm can be transmitted and initiate indoor photochemistry, raising the possibility of elevated radical concentrations indoors and subsequent oxidation of VOCs.[12−14] While other photolytic radical sources require UV light at shorter wavelengths, HONO can be a primary source of OH radicals indoors since it photolyzes at longer wavelengths (R1) and has indoor sources resulting in elevated HONO concentrations compared to outdoors.[15]

$$\mathrm{HONO} + h\nu \xrightarrow{\lambda < 400\ \mathrm{nm}} \mathrm{OH} + \mathrm{NO} \qquad \text{(R1)}$$

Human activities (e.g., cooking, cleaning) can alter the composition of the indoor atmosphere. Gas stoves are a known source of nitric oxide (NO) and nitrogen dioxide (NO_2), collectively known as NO_X, as well as HONO.[16−19] These reactive species not only provide a potential source of OH radicals through HONO photolysis but can also (a) propagate the radical cycle through reactions of NO with peroxy radicals produced by the reaction of OH with VOCs (denoted by RH, reactions R2−R4) as well as (b) terminate the cycle via the reaction of OH with NO_2 (R5R5).[20] The oxidation of VOCs by OH leads to the production of oxygenated VOCs (R′O in R3R3), which can lead to secondary organic aerosol formation and potentially impact human health.[21,22]

$$\mathrm{OH} + \mathrm{RH} \xrightarrow{\mathrm{O_2}} \mathrm{RO_2} + \mathrm{H_2O} \qquad \text{(R2)}$$

$$\mathrm{RO_2} + \mathrm{NO} \xrightarrow{\mathrm{O_2}} \mathrm{R'O} + \mathrm{HO_2} + \mathrm{NO_2} \qquad \text{(R3)}$$

Received: August 9, 2022
Revised: December 8, 2022
Accepted: December 12, 2022
Published: January 5, 2023

$$HO_2 + NO \rightarrow OH + NO_2 \quad (R4)$$

$$OH + NO_2 \xrightarrow{M} HNO_3 \quad (R5)$$

Only three previous studies have directly measured concentrations of OH in indoor environments. Measurements in a classroom found OH concentrations as high as 1.5×10^6 molecules/cm^3.[23,24] In comparison, typical outdoor concentrations of OH reach a maximum of $2-10 \times 10^6$ molecules/cm^3 at midday.[25] The elevated indoor OH concentrations occurred both when the windows were opened as well as when the room received direct sunlight while windows were closed. Steady-state comparisons and modeled analysis posited that the main source of OH was the photolysis of HONO.[23,24] In a second study, OH concentrations of 4.0×10^6 molecules/cm^3 were measured in a classroom during a cleaning episode using limonene, a common ingredient in lemon-scented cleaners and a source of radicals upon its reaction with O_3. The ambient concentration of OH increased to 1.8×10^7 molecules/cm^3 when an air-cleaning device was operated near the sampling instrument.[26] A third, recent study focused on the effect of different VOC concentrations from painted surfaces on indoor radical concentrations. OH was measured at $6-10 \times 10^5$ molecules/cm^3 in direct sunlight, in good agreement with a zero-dimensional model.[27]

In this study, measurements of OH were conducted near a window during several cooking experiments during the House Observations of Microbial and Environmental Chemistry (HOMEChem) campaign. While these measurements may not be characteristic of the average household concentration due to the short lifetime of OH,[28] the observed concentrations of OH were compared to the results of a chemical model to determine whether known radical sources such as HONO could explain the observed OH radical concentrations. Interferences associated with the measurements of NO_2 and O_3 during cooking episodes were also analyzed to determine whether unmeasured VOCs may be responsible for the observed interferences and potentially contribute to the production of radicals during indoor cooking events.

2. EXPERIMENTAL METHODS

2.1. HOMEChem Study. The HOMEChem campaign was a collaborative study designed to investigate the chemical transformations in a residential environment during a variety of realistic household events. The campaign took place during June 1−28, 2018, in a previously unoccupied, 111 m^2 manufactured home located on the J. J. Pickle Research Campus of the University of Texas, Austin. The fan in the AC system operated continuously to provide consistent mixing within the house throughout the campaign at an equivalent rate of 8 h^{-1}. The house thermostat controlled the indoor temperature at 25 °C by turning on and off the condenser and cooling coil of the AC system. As the AC did not provide outdoor air, a dedicated ventilation system was installed and provided constant outdoor air supply to the house. The air change rate (ACR) was continuously monitored and averaged 0.5 ± 0.1 h^{-1} throughout the whole campaign when the doors and windows were closed.

While the HOMEChem campaign involved a variety of cooking, cleaning, and other experiments,[29] here, we focus on two cooking experiments: the 12 June experiment featuring repeated, stir-fry cooking events, and the 27 June experiment replicating a traditional American Thanksgiving. Replications of these experiments were also done, but the 12 June and 27 June days represent the most comprehensive data required to constrain the model. On 12 June, the first cooking episode used an electric hotplate, while the next three used a single burner of the propane gas stove to cook the same meal. After the first two trials, the house was extensively ventilated by opening all windows and doors for 30 min approximately 1 h after the cooking event ended. The final cooking trial occurred after sunset. In each trial, three volunteers would enter the house, cook, eat, and then leave so that the house was unoccupied between trials. During the 27 June Thanksgiving experiment, the gas burners and oven were used as needed, and at times, all four burners and the oven were on simultaneously. There were no dedicated ventilation periods, rather four volunteers entered in the morning to cook, then nine others entered in the afternoon to eat and clean before everyone left around 17:00, local time.

Several instruments were used to characterize the indoor environment, with locations shown in Figure S1 and summarized in Table S1. Overall, instrumentation was centered around the kitchen, where the majority of emissions occur. However, the instrument size and logistical restrictions prevented all instruments from being located in the kitchen. To reduce concentration gradients, the AC fan was run continuously, regardless of heating and cooling, mixing the indoor air at a rate of 2000 m^3 h^{-1} and resulting in a well-mixed environment for compounds with a lifetime greater than 20 min. NO and NO_2 were measured using a Thermo Fisher model 42i TL monitor with a home-built blue light converter (BLC) for the detection of NO_2. NO_2 was also measured using a cavity attenuated phase shift (CAPS) instrument from Environnement S. A. O_3 was measured using a 2BTech model 202 instrument sampling near the kitchen (hereafter KIT O_3) and also using a Horiba APOA 370 instrument sampling from before the cooling coiling of the AC within the air handling unit (hereafter AHU O_3). As the AC provided no ventilation and only recirculation, concentrations from the AHU O_3 represent the indoor air concentration. Polytetrafluoroethylene (PTFE) filters were used to prevent particulate matter interferences with gas-phase measurements. VOCs were measured with a custom 4-channel gas-chromatograph (GC),[30] a proton transfer reaction-time of flight-mass spectrometer (PTR-MS, Ionicon Analytik GmbH, Austria, PTRTOF 8000), and a chemical ionization mass spectrometer (CIMS, Tofwerk AG and Aerodyne Research Inc.) paired with iodide chemical ionization with inlets located in the kitchen. Photon flux from windows was measured with an Ocean Optics USB4000 spectrometer equipped with a cosine corrector.[31] This spectrometer was located on top of the OH instrument for the two cooking episodes examined. Photon fluxes were used to calculate photolysis rates of relevant indoor species. Concentrations of OH and photon fluxes likely exhibited gradients due to the short lifetime of OH and the large difference between indirect and direct sunlight. Because of this, they were co-located near the window so modeled OH concentrations could be compared to measurements. HONO was measured using another CIMS (Tofwerk AG and Aerodyne Research Inc.) instrument paired with acetate chemical ionization[32] sampling from an inlet in the kitchen and also measured in the living room by a custom-built laser-photofragmentation laser-induced fluorescence (LP/LIF) instrument.[33]

https://doi.org/10.1021/acs.est.2c05756
Environ. Sci. Technol. 2023, 57, 896−908

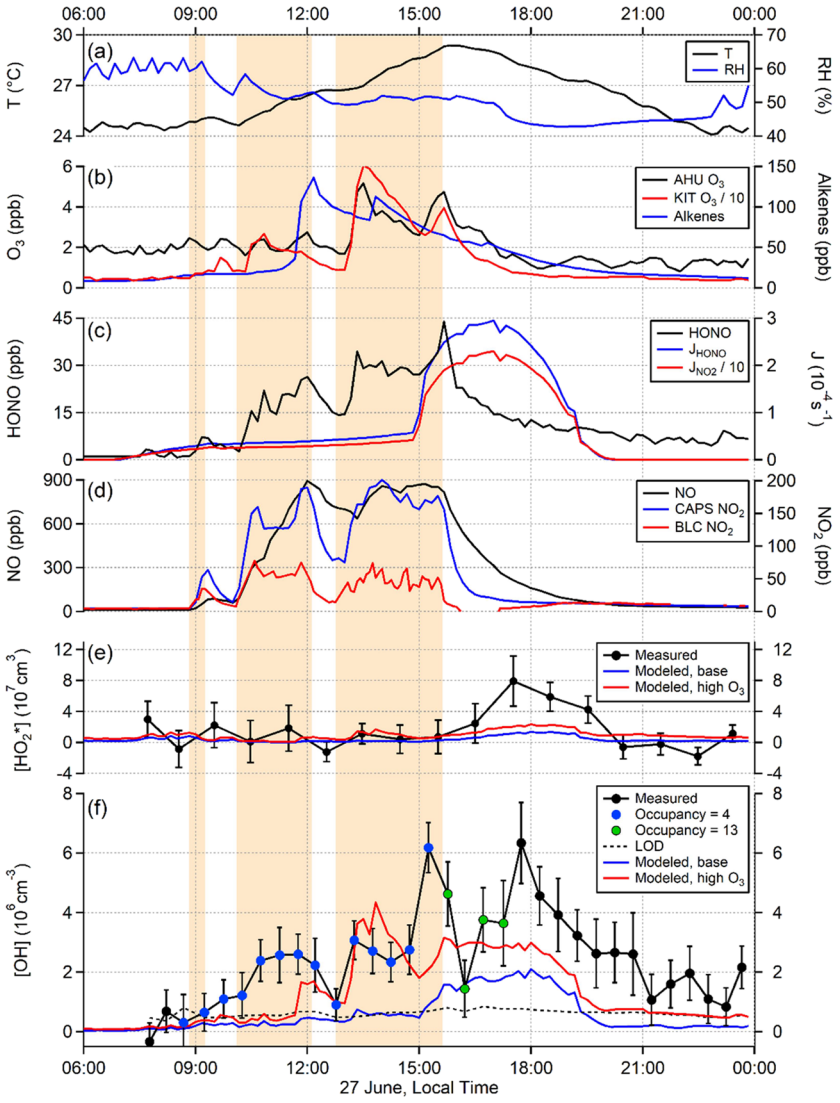

Figure 1. Measurements from the 27 June Thanksgiving experiment. Orange-shaded regions indicate periods of gas cooking. (a) Temperature and relative humidity (b) alkene concentrations and both O_3 instruments, with the KIT O_3 divided by 10, (c) HONO and J_{HONO}, (d) NO and both measurements of NO_2, (e) measured HO_2* and modeled HO_2 concentrations from the base and high O_3 scenarios (see text), and (f) measured and modeled OH concentrations from the base and high O_3 scenarios. Green points in (f) indicate a period of increased human activity near the OH instrument, potentially creating a local OH sink or sink of photolytic precursors resulting in lower concentrations.

2.2. Measurements of Radicals during HOMEChem. OH radicals were measured using a laser-induced fluorescence instrument which has been described in detail elsewhere.[33] In this technique, OH radicals are detected after ambient air is sampled through a pinhole inlet into a low-pressure cell (approximately 0.26 kPa). The detection cell was located in front of the westward-facing living room window, while much of the chemically active emissions came from the kitchen, approximately 5.5 m away.

A separate detection axis was deployed to measure HO_2. In this instrument, the addition of NO within the low-pressure detection cell converts HO_2 into OH through R4R4. The OH is then detected by laser-induced fluorescence. This technique is susceptible to interferences from peroxy radicals (RO_2) derived from the OH-initiated oxidation of alkenes and aromatics, as these radicals can be quickly converted to HO_2 (and subsequently OH) upon reacting with NO (R3R3).[34] Because of this interference, measurements of peroxy radicals are denoted as HO_2*, defined as the sum of HO_2 plus a fraction of interfering RO_2 radicals, and represent an upper limit to the actual HO_2 concentration.

In a trailer next to the test house, a tunable dye laser (Sirah Credo) pumped by the second harmonic of a Spectra Physics Navigator II YHP40-532 Nd-YAG laser produced approximately 40 mW of radiation at 308 nm at a repetition rate of 10 kHz. A portion of the laser emission was transmitted to the detection cells inside the test house via 12 m optical fibers (ThorLabs), resulting in approximately 2−6 mW within each cell. The OH fluorescence in each axis is temporally separated from the laser excitation occurring at the same wavelength and is detected with a gated microchannel plate photomultiplier tube (Photek PMT325). To distinguish the OH fluorescence from background signals such as scatter from the laser that extends into the gated detection window, the laser wavelength is varied on- and off-resonance with the $Q_1(3)$ transition of OH at 308.1451 nm through spectral modulations. The net OH fluorescence signal is derived by the subtraction of the off-resonant signal from the resonant signal.

https://doi.org/10.1021/acs.est.2c05756
Environ. Sci. Technol. 2023, 57, 896−908

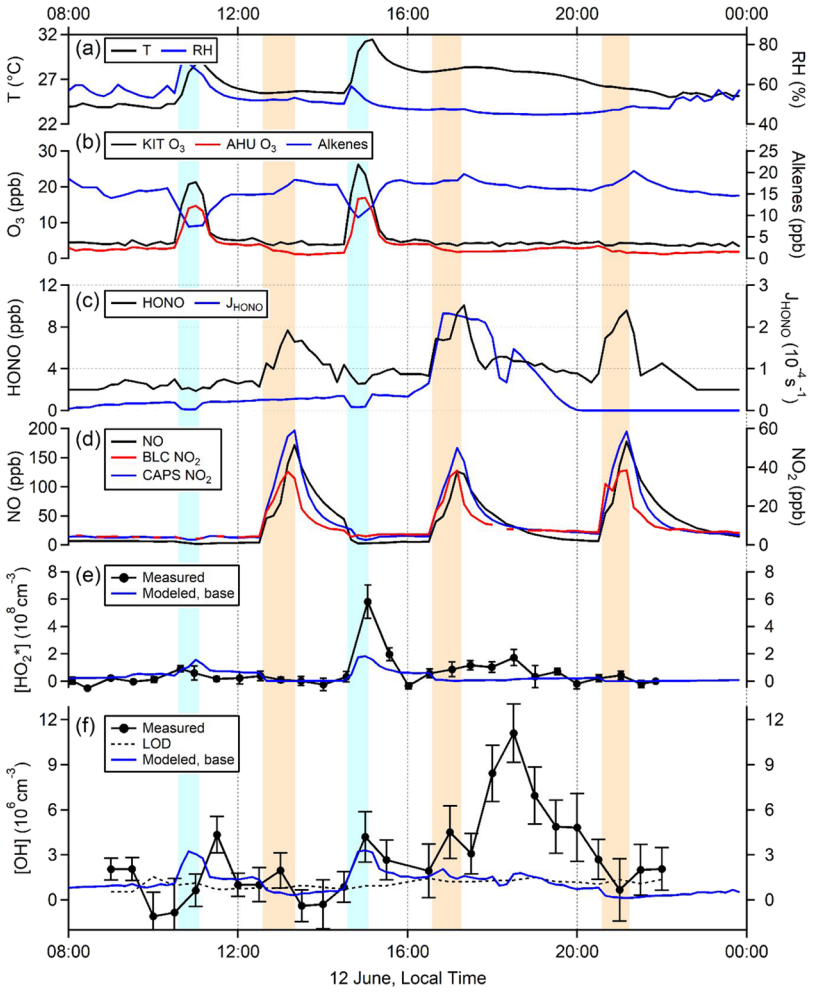

Figure 2. Measured concentrations and environmental parameters for the 12 June repeated cooking events. Measurements include temperature, relative humidity (a), O_3, alkenes (b), HONO, light (c), NO, NO_2 (d), HO_2* (e), and OH (f). Modeled concentrations from the base model are also shown in (e, f). Blue-shaded regions indicate ventilation periods while orange-shaded regions indicate the use of the gas stove.

The sensitivity of the instruments to OH is calibrated intermittently throughout the campaign using the photolysis of water vapor at 185 nm as an OH source, as described previously.[35] The OH instrument had a limit of detection (1σ) of approximately 6.2×10^5 and 1.2×10^6 cm^{-3} for the Thanksgiving and repeated cooking experiments, respectively (S/N = 1, 30 min average). The uncertainty associated with the UV water photolysis calibration technique is estimated to be ±18% (1σ).[35] The conversion efficiency of HO_2 to OH is determined by adding NO to the OH calibration source, as the photolysis of water vapor produces equal quantities of OH and HO_2.[35]

2.3. Modeling OH Concentrations. The measured OH concentrations were modeled using a zero-dimensional chemical box model with the Regional Atmospheric Chemistry Mechanism v.2 (RACM2)[36] in the Framework for 0-D Atmospheric Modeling (F0AM).[37] The model was constrained with measurements of VOCs, NO, NO_2 (from CAPS), O_3, and measured photolysis frequencies. A list of all VOCs used to constrain the model is included in Table S2. The model OH concentrations were not sensitive to VOC concentrations, and increasing or reducing total VOC concentrations by a factor of two did not result in a difference greater than the model error of ±15%. All constrained compounds had lifetimes longer than 20 min and are likely to be well-mixed within the house. Since the photolysis frequencies were measured at the same location as the OH measurements, this model should simulate the concentration of OH near the window rather than a household average. To account for heterogeneity in photolysis with direct and indirect light coming in through windows (in addition to artificial light), the measured photolysis frequencies under indirect light were doubled in the model, similar to that done previously.[23,38] As a result, the modeled OH concentrations during periods of indirect light (i.e., before 15:00) represent an upper limit. To account for transport between the indoor and outdoor environments, a loss pathway with a rate equal to the air change rate of the house (approximately 0.5 h^{-1}) was applied to all chemical species in the model. While point sources, such as the gas stove, could introduce gradients in concentration that would not be captured in 0-D modeling, the continuous operation of the fan in the AC system provided constant mixing and minimized concentration gradients.

3. RESULTS AND DISCUSSION

3.1. Measurements and Model Constraints. Figure 1 shows the measured ambient concentrations of relevant species and environmental parameters for the 27 June Thanksgiving experiment. The temperature and relative humidity (RH; Figure 1a) were largely controlled by the AHU of the AC and cooling coil on−off operation, which was running throughout

https://doi.org/10.1021/acs.est.2c05756
Environ. Sci. Technol. 2023, 57, 896−908

the day. AHU O_3 concentrations were typically below 5 ppb during the day. In contrast, KIT O_3 displayed a significant interference leading to reported mixing ratios as high as 60 ppb (Figure 1b). AHU O_3 may have been affected by the same interference, as the observed increase to 4 ppb in the afternoon (13:00−16:30) is unlikely, given the high concentration of NO present at this time (approximately 900 ppb). This interference will be discussed further in Section 3.4.

The alkene mixing ratios shown in Figure 1b represent a subset of all VOC measurements and indicate emissions during cooking. The majority of alkenes measured were monoterpenes (Figure S2) and the two peaks in the day (150−100 ppb) correspond to particularly fragrant events (i.e., cutting citrus fruits at 11:50 and cooking celery, onion, carrots, and sage at 14:00). The HONO and NO_2 photolysis rate constants (J_{HONO} and J_{NO2}, Figure 1c) clearly indicated the presence of direct light on the LIF instruments from the west-facing window from 15:00 until sundown as the spectrometer was located in the living room near the LP/LIF instrument. From sunrise until 15:00, indirect light was present in the living room from both the west-facing window in the living room and the east-facing window in the kitchen. The measured spectral irradiance from the west-facing window is shown in Figure S3. NO, NO_2 (Figure 1d), and HONO (Figure 1c) increased whenever the gas stove was in use.[39,40] The NO_2 concentration measured by the CAPS instrument was significantly higher than the NO_2 concentration measured by the BLC monitor. This discrepancy will be further discussed in Section 3.5.

HO_2* concentrations (Figure 1e) reached a peak of 1.2×10^8 molecules/cm^3 at 18:00, during the period of direct sunlight. This peak also coincides with the decrease in NO, which represents a major sink of HO_2. Measured OH concentrations (Figure 1f) were above the limit of detection of the instrument for most of the day. Measured concentrations in the morning were approximately 2×10^6 molecules/cm^3, increasing to approximately 6×10^6 molecules/cm^3 at 15:15 when direct sunlight begins to illuminate the living room area through the west-facing window. Due to the decreasing HONO concentrations, this peak also corresponds to the highest value of $J_{HONO} \times [HONO]$. The measured OH concentration decreased between 15:35 and 17:00 (green points in Figure 1f), when thirteen people were present. During this time, the bulk of the activity also moved from the kitchen into the living room, nearer to the OH instrument. A recent study has shown that under low O_3 conditions, the surfaces of skin and clothing can act as a radical sink.[41] It is possible that this introduced new heterogeneity in VOC concentrations and radical sinks resulting in a greater loss of OH or any radical precursors nearer the instrument than can be accounted for by the measured VOC concentrations sampled from the kitchen. After people left the house at 17:00, OH returned to its previous concentration of about 6×10^6 molecules/cm^3 likely due to the removal of radical sinks adjacent to the instruments. The OH concentration then began slowly decreasing while remaining above the limit of detection of the instrument until the end of the day. Modeling results (discussed in Sections 3.2 and 3.6) are also shown in Figure 1e,f.

These same chemical species and environmental parameters for the 12 June repeated cooking experiments are shown in Figure 2. Many of the same trends can be seen on this day, with relatively lower concentrations of HONO (Figure 2c), NO, and NO_2 (Figure 2d) due to the reduced use of the gas stove compared to the Thanksgiving experiment. The ventilation periods can be clearly seen in temperature, RH (Figure 2a), and O_3 concentrations (Figure 2b). During these times, the air conditioner was turned off resulting in an increase in temperature, while the fan remained on to maintain air flow through the house. O_3 significantly increased during ventilation periods due to the higher ambient concentration outside. Otherwise, O_3 concentration remained stable through the day. A noticeable peak in HO_2* at 15:00 coincides with the ventilation period, potentially due to increased infiltration of outdoor HO_2 or increased concentrations of O_3, a radical precursor. Unlike the Thanksgiving experiment, OH remained at or below the limit of detection throughout the morning period and only rose to significant concentrations in the afternoon and evening, when the instrument was illuminated by sunlight through the westward-facing windows, peaking at approximately 18:30. Observations from the other cooking events are shown in Figures S4−S6.

3.2. Base Model Predictions of OH Concentrations. Initial modeling results of the 27 June Thanksgiving experiment using both the KIT O_3 and AHU O_3 measurements to constrain the O_3 concentration are shown in Figure 1e,f. Due to the significant interference with the KIT O_3 measurements (discussed in Section 3.4), the model using the AHU O_3 measurements is considered the base model for this day (blue line, Figure 1e,f). This model underestimates OH concentrations, with a median observed-to-modeled ratio of 5.0 (quartiles = 2.9, 7.5). The modeled HO_2 is also substantially lower than the measured HO_2*, although modeled concentrations should be considered a lower limit, as they do not include any RO_2 interference. Recent studies have suggested that other photodegradable or photolabile compounds in secondary organic aerosols are not included in models and may greatly impact radical production rates.[42−44] An unmeasured or unmodeled photolytic species could increase the modeled OH concentrations and improve agreement with measurements.

Constraining the model with the KIT O_3 (red line, Figure 1e,f) recreates the observed OH concentrations better than the base model due to enhanced radical production from alkene ozonolysis (66% of total radical sources) and unreasonably high O_3 concentrations. The high-O_3 model had a median observed-to-modeled ratio of 1.9 (quartiles = 1.4, 3.2). The ability of this model to capture the early afternoon trends of OH, including the brief pause in cooking around 13:00, suggests that there may be a link between the interference in the ozone measurements and the disagreement between measured and modeled OH concentrations in the base model. This is indicative of either missing radical sources in the model, an interference in the OH measurements, or some combination of both.

3.3. Analysis of Potential Interferences with the OH Measurements. Several potential interferences have been reported for some LIF instruments, including laser-generated interferences and degradation of organic trioxides and Criegee intermediates.[11,45−48] Laser-generated interferences include the photolysis of O_3 by the laser, leading to the production of excited oxygen atoms which can react with water vapor to artificially produce OH in the detection cell (Equations R6a,b). This interference was calibrated in the laboratory before and after HOMEChem by sampling air with varying concentrations of water vapor and O_3. Expected signals from O_3 photolysis within the cell did not exceed the limit of detection of the instrument. Any uncalibrated laser-generated interferences

https://doi.org/10.1021/acs.est.2c05756
Environ. Sci. Technol. 2023, 57, 896−908

should correlate with laser power. However, as shown in Figures 3d and S7, there is actually an anti-correlation for 27 June and no correlation on 12 June, so it is unlikely that any laser-generated interferences affected the measurements.

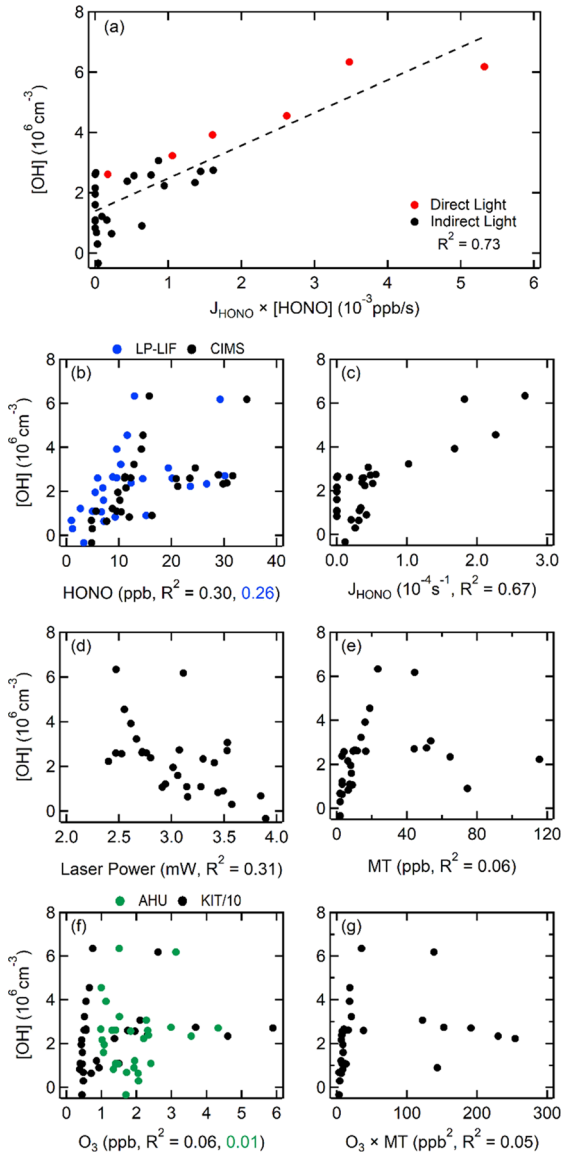

Figure 3. Measured OH concentrations plotted against indoor sources (a) and indications of potential LP/LIF instrument interferences (HONO (b), J_{HONO} (c), laser power (d), monoterpenes (e), O_3 (f), and the product of O_3 and monoterpenes (g)) during the 27 June Thanksgiving experiment. Points when guests arrived (15:30−17:30) were omitted. The strong correlation with HONO photolysis compared to weak correlations with interference precursors suggest that the measurements do not suffer from interferences. In panel a, J_{HONO} × [HONO] was calculated using LP/LIF values for HONO.

$$O_3 + h\nu \rightarrow O_2 + O(^1D) \quad \text{(R6a)}$$

$$O(^1D) + H_2O \rightarrow 2OH \quad \text{(R6b)}$$

Criegee intermediates, formed from the reaction between O_3 and alkenes, and organic trioxides (ROOOH) produced from the reaction of OH with RO_2 radicals, could decompose inside the low-pressure detection cell to produce OH.[11,45,48] These and any other potential interference can be measured using chemical modulations through the addition of a chemical scrubber such as hexafluoropropene (C_3F_6) just above the inlet to remove ambient OH. Any OH signal that is measured when the scrubber is added is due to OH that is generated inside the detection axis. However, to avoid contaminating the indoor environment during HOMEChem, chemical modulations were not used to measure potential interferences. Instead, the OH concentrations were compared to a primary indoor OH source (HONO photolysis) as well as precursors of Criegee intermediates, such as monoterpenes and ozone, as shown in Figure 3 for 27 June and Figure S7 for 12 June. In Figure 3a, the OH concentrations are correlated to J_{HONO} × [HONO] (R^2 = 0.73), suggesting that the source of OH is photolytic. This includes periods when direct sunlight was illuminating the living area, as well as periods when indirect light was illuminating the area. In contrast, the measured OH concentrations were not correlated with the measured HONO concentrations from the CIMS or LP/LIF instruments, suggesting that potential interferences from elevated HONO concentrations, such as photolysis by the 308 nm laser in the detection cell, were not responsible for the measured OH concentrations.

If the measured OH concentrations were the result of interferences from the decomposition of Criegee intermediates produced from the ozonolysis of alkenes, one would expect that the measured OH concentrations would exhibit some correlation with the measured concentrations of ozone and reactive VOCs emitted during the cooking episodes. As illustrated in Figure 3e−g, there is little or no correlation of the measured OH concentrations with VOCs that react with ozone, such as monoterpenes (MT) or the product of ozone with these VOCs reflecting the rate of ozonolysis, indicating that the OH measurements are probably free from interferences due to the decomposition of Criegee intermediates in the detection cell. The measurements are also likely free from interferences from the decomposition of organic trioxides in the detection cell as the high concentration of NO likely dominated the fate of peroxy radicals in these experiments.

The correlation of the measured OH concentrations with J_{HONO} × [HONO] during the cooking episodes suggests that the source of OH is related to the photolysis of HONO. There is also a correlation with J_{HONO} alone (Figure 3c), implying that the main production route of OH is photolytic, as the photolysis frequencies for all compounds will scale similarly. During Thanksgiving, the correlation of J_{HONO} × [HONO] is greater than that of either J_{HONO} or [HONO], suggesting that the photolysis of HONO is likely a dominant source. The lower concentrations of HONO during the repeated cooking experiment resulted in comparable correlations between J_{HONO} and J_{HONO} × [HONO]. The correlation to J_{HONO} × [HONO] would also be consistent with the photolysis of an unmeasured radical source co-emitted with HONO during the cooking episodes. As discussed below, interferences observed by some of the instruments measuring ozone and NO_2 indicate the presence of a photolytic source of radicals during the cooking episodes that could contribute to the measured OH concentrations. Because the measured OH concentrations are not correlated to the KIT O_3 (Figure 3, R^2 = 0.06) or the difference between NO_2 measurements (R^2 = 0.07, not shown), interferences in these instruments are unlikely to indicate an interference in the OH measurements.

https://doi.org/10.1021/acs.est.2c05756
Environ. Sci. Technol. 2023, 57, 896−908

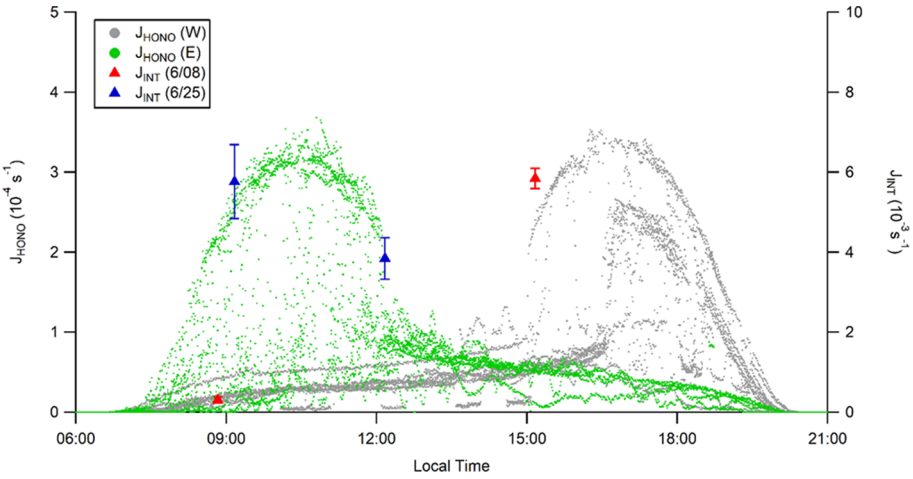

Figure 4. Calculated photolysis frequencies of the interfering species (J_{INT}, right axis) based on measurements during 8 June (red points) and 25 June (blue points) with all of the measured J_{HONO} values from the entire campaign (small dots, left axis) as a function of time of day. Bimodal distribution is due to individual measurements from the two main windows, one facing east in the kitchen (green dots) and one facing west in the living room (gray dots).

3.4. Evidence of Photolabile Interference in Ozone Instruments. Figures 1b and S8 show the measurements by the KIT O_3 instrument with the measurements by the AHU O_3 instrument during the 27 June Thanksgiving experiment, illustrating the large discrepancy between the two instruments. The calculated steady-state concentration of O_3 and the measured concentrations of both instruments are also shown in Figure S8. The consistently high concentrations of the KIT O_3 instrument clearly suggest an interference, which may also have affected the AHU O_3 instrument with the increase from 13:00 to 17:00 occurring during a marked decrease in the calculated steady-state O_3 concentration due to the high NO concentrations during this period. While both instruments measure O_3 through its absorbance at 254 nm (see Supporting Information), it is possible that the interference is lost within the air conditioning system, similar to water-soluble trace gases.[49] This would result in a lower interference in the AHU O_3 measurements compared to the KIT O_3 measurements.

Discrepancies between the two O_3 instruments also occurred on three other days during the HOMEChem campaign, all during cooking events (8 June, 25 June, and 26 June, Figure S9). The interference in the KIT O_3 measurements exhibited an exponential decay after each episode, allowing the calculation of the total decay rate constant (Figure S10). The 26 June cooking event took place at night and exhibited a slower decay than the daytime events ($k = 1.15 \times 10^{-3}$ s^{-1} compared to $1.45-6.99 \times 10^{-3}$ s^{-1}, Figure S10), suggesting that the interference is photolytic, resulting in a shorter lifetime during the day. With the assumption that all other decay pathways remain relatively similar between different days, the photolysis rate constant of the interferent can be calculated by subtracting the total decay rate constant calculated at night from the total decay rate constant calculated from each day (see the Supporting Information). This provides an approximate rate constant for the photolysis of the interferent (J_{INT}) averaged throughout the house during four different times of the day; however, this calculation is highly uncertain because it is based on the assumption that all other loss pathways are constant. The results are shown in Figure 4 overlaid with measurements of J_{HONO} measured from both the east- and west-facing windows throughout the campaign showing the diurnal trend of sunlight in the house. There is a substantial difference between the interference J-values calculated around 9:00 on the two days, when the house usually received direct sunlight from the eastern window. Unfortunately, photolysis rates from the east-facing window were not measured on 8 June. The reason for this discrepancy is unclear and may be due to either uncertainty associated with the calculation or uncertainties related to the amount of local cloud cover on that day (see the Supporting Information). While these calculated photolysis frequencies are highly uncertain due to their reliance on assumptions, they do suggest that the interfering compound is most likely photolytic in the indoor environment.

Ozone instruments have known interferences with aromatic species, HONO, and aldehydes,[50−53] but concentrations of these species measured during HOMEChem can only account for a maximum increase in the signal of 1 ppb (Figure S11). Other classes of compounds, such as polycyclic aromatic hydrocarbons, could absorb at 254 nm,[54] but were not measured. As O_3 absorbs very strongly at 254 nm compared to these interfering compounds, to account for a difference in O_3 signal of more than 50 ppb, interferences would have to be present in high concentrations. Nevertheless, if the absorption cross-section of the interference at 254 nm was much larger than that of other known interferences, then smaller concentrations could explain the observed interference.

3.5. Evidence of Photolabile Interference in NO_2 Instruments. The instruments that measured NO_2 during the campaign used two different techniques (BLC and CAPS) with inlets located adjacent to one another within the house during experiments. Any discrepancy between the two instruments could be due to calibration differences or an interference in one of the techniques. Throughout the campaign, the BLC instrument measured higher values at low concentrations of NO_2 compared to the CAPS instrument, while the CAPS instrument measured higher values compared to the BLC instrument at high concentrations (Figure S12). There are also periods of substantial discrepancies with negative BLC NO_2 concentrations, clearly indicative of an interference. An interference photolyzing into a compound that quickly reacts with NO (such as the hydroperoxy radical (HO_2) or a peroxy radical, RO_2) would decrease the NO_2

https://doi.org/10.1021/acs.est.2c05756
Environ. Sci. Technol. 2023, 57, 896−908

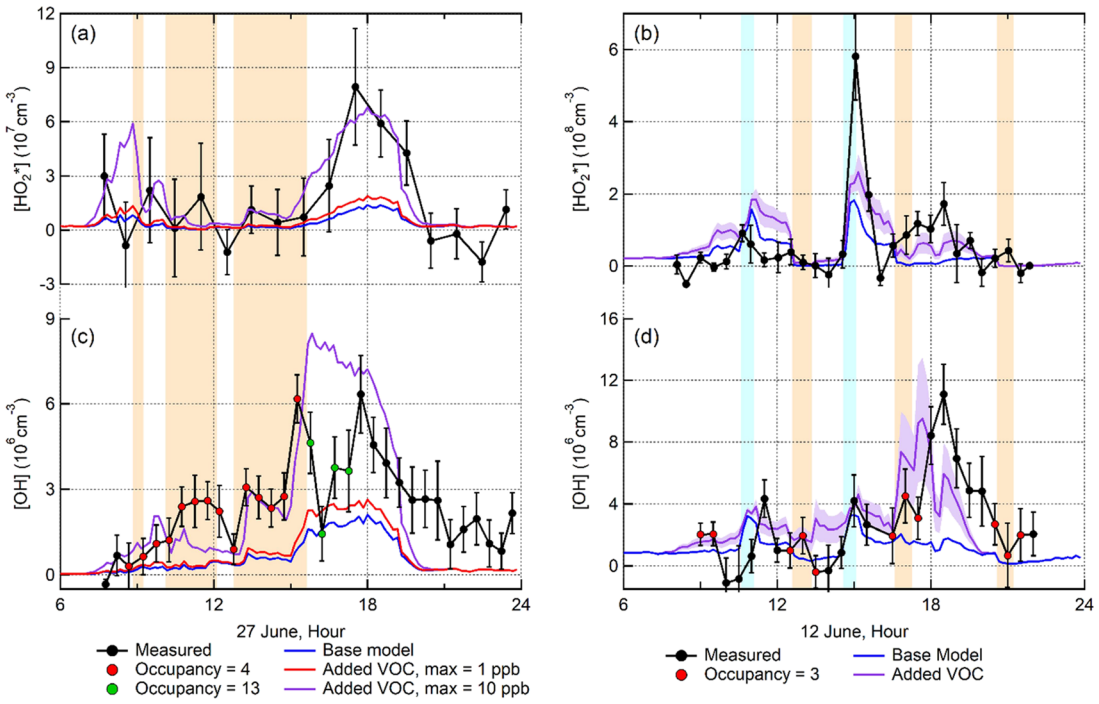

Figure 5. Measurements of HO_2* (a and b) and OH (c and d) during cooking events. Model results for the base case (blue) and with an additional photolytic VOC with a maximum concentration of 1 ppb (red) and 10 ppb (purple) for the 27 June Thanksgiving experiment (a and c) and the 12 June Repeated Cooking event (b and d). Variations in the concentration of the photolytic VOC were scaled to the difference in signals between the O_3 instruments for the Thanksgiving experiment, and the ratio of interference/NO_2 was subsequently used to constrain the 12 June model (see text). Occupancy of the house is indicated by the color of the points, with red points when 3−4 people were present, green points with 13 people present, and unoccupied times in black points. The shading of the 12 June model represents a model run with the photolytic VOC changed by ±50%.

signal when the BLC is active by reducing the detected NO in the NO+NO_2 signal, while not affecting the ambient NO signal when the BLC is off, resulting in a NO_X signal that is smaller than NO.[29,55] The interference was greatest during exceptionally high NO_X events such as the Thanksgiving experiments, leading to negative signals when NO was greater than NO_2, but could also be present at elevated NO_X concentrations, such as the 12 June repeated cooking experiment, leading to lower NO_2 signals compared to the CAPS instrument.

If an interference is present in the BLC NO_2 measurements, it must be distinguished from any differences from the CAPS measurements due to calibration uncertainties. With the assumption that the interference is tied to emissions from the gas stove, one experiment during the campaign featured elevated NO_2 concentrations without the use of the gas stove or any other combustion sources through the addition of O_3 inside the house. The O_3 reacted with NO to form NO_2, resulting in elevated concentrations of NO_2 in the absence of combustion and presumably no interference. During this experiment, the measurements by the two instruments were highly correlated but did diverge at both low and high mixing ratios of NO_2 (Figure S13), suggesting that the difference was due to calibration uncertainties during this experiment. Assuming that this systematic difference between the instruments was consistent throughout the campaign, the linear relationship between the two instruments on this day can be used to correct the BLC measurements on other days so that any remaining discrepancy with the CAPS instrument is assumed to be due to the interference. This discrepancy is significant during the Thanksgiving experiment (Figure 1d) but also noticeable on repeated cooking days, as shown in Figure S14, suggesting that the interference was emitted during all cooking events.

Quantification of the interference in the NO_2 instrument is inherently challenging due to two reasons. First, the photolytic efficiency of the interfering species is unknown. To interfere with NO_2 measurements, the species would need to absorb and photolyze at 395 nm. As blue light converters use wavelengths at particularly high absorbance cross-sections of NO_2, any interfering species will likely have a lower absorbance and lower rate of photolysis. Therefore, determining the difference between the two signals would only account for the fraction of the interfering species that photolyzes and would represent a lower limit. Second, if the compound reacting with NO is a peroxy radical, there is a possibility that the radical cycle continues to propagate and each interfering RO_2 molecule can cause the loss of multiple NO molecules in the instrument. As a result, the difference between the two NO_2 concentrations could represent the upper limit of the interference concentration.

3.6. Model Results with an Additional Photolytic Source of Radicals. To examine the effect of an unmeasured or under-measured photolytic source of radicals during the Thanksgiving experiment, an additional VOC was added to the 0-D model. The photolysis pathway of this VOC was modeled after pyruvic acid ($CH_3C(O)C(O)OH$, reactions R7−R10), while the total photolysis frequency was scaled to match the calculated values shown in Figure 4. Pyruvic acid was chosen as the proxy in the model for four reasons. (1) Organic acids are commonly found in food, including many cooked food during Thanksgiving,[56,57] (2) the concentration of pyruvic acid measured during the Thanksgiving experiment was correlated

https://doi.org/10.1021/acs.est.2c05756
Environ. Sci. Technol. 2023, 57, 896−908

to the KIT O_3 measurements (Figure S15), (3) it can absorb at 254 nm and interfere with the O_3 instrument, and (4) it absorbs up to 400 nm and can photolyze to form peroxy radicals which would interfere with the NO_2 instrument. While pyruvic acid was measured during the HOMEChem campaign by the iodide chemical ionization mass spectrometer (I-CIMS), including the concentration measured during the Thanksgiving experiment in the model does not impact the modeled radical concentrations greater than the model error of ±15%. However, the I-CIMS instrument was not specifically calibrated for pyruvic acid against a standard but was rather calibrated for formic acid, acetic acid, propionic acid, butyric acid, valeric acid, hypochlorous acid, chlorine, and nitryl chloride. The mixing ratios of all other compounds were estimated using a voltage scanning approach as described in Lopez-Hilfiker et al.[58] and Mattila et al.,[59] resulting in a high uncertainty for all uncalibrated compounds, including pyruvic acid. Because of this, it is possible that the instrument is not as sensitive to pyruvic acid or that pyruvic acid could have been lost on sample lines. Both possibilities could indicate a higher true concentration of pyruvic acid inside the house compared to the measured concentration. Additionally, although the proxy is a single compound, it could represent the sum of many functionalized, photolytic compounds emitted from cooking, each contributing to the total rate of radical production.

$$CH_3C(O)C(O)OH + h\nu \rightarrow CH_3CHO + CO_2 (\phi = 0.48) \quad \text{(R7)}$$

$$CH_3C(O)C(O)OH + h\nu \rightarrow CH_3CO + COOH\ (\phi = 0.39) \quad \text{(R8a)}$$

$$COOH + O_2 \rightarrow HO_2 + CO_2 \quad \text{(R8b)}$$

$$CH_3C(O)C(O)OH + h\nu \rightarrow CH_3COOH + CO\ (\phi = 0.08) \quad \text{(R9)}$$

$$CH_3C(O)C(O)OH + h\nu \rightarrow CH_3CO + CO + OH\ (\phi = 0.05) \quad \text{(R10)}$$

For the Thanksgiving experiment, the concentration of the additional radical source used in the model was scaled to the difference in signals between the two O_3 monitors during the day, with the maximum concentration varied to obtain the best match between the modeled OH concentrations and the measurements (Figure S16). The results for both the base model and the model including the additional radical source are shown in Figure 5, and a radical budget analysis can be found in the Supporting Information (Figure S17). Scaling the expected photolysis rate constant for pyruvic acid to the measured J_{INT} and assuming a maximum indoor concentration of the photolytic VOC of 1 ppb increases the modeled OH concentration by 10% over the base model during indirect sunlight (11:50−13:00) and 35% during direct sunlight (13:30−18:00). However, with this additional photolytic VOC, the model still underestimates the measured OH concentrations. Increasing the maximum concentration of the photolytic VOC to 10 ppb (Figure 5, purple line) using the same photolysis rate constant improves the agreement of the modeled OH concentrations with the measurements, leading to a median observed-to-modeled ratio of 1.3 (quartiles = 0.71, 3.6). This model also improved the agreement between the measured HO_2* and modeled HO_2 during the evening peak around 17:00. While the models were unable to capture the elevated OH concentrations in the morning (10:30−12:00) or late in the evening (20:00−0:00), the additional photolytic VOC was able to bring the model into better agreement for most of the time when the interference concentration was high or when the evening light was coming through the west-facing window. Differences in the absorption cross-section between pyruvic acid and the unknown photolytic VOC could be responsible for some of the discrepancies between the modeled and measured OH concentrations in the morning and early evening. The discrepancy could also be due to additional radical production from the ozonolysis of alkenes that were not included in the model.

The repeated cooking experiment on 12 June also displayed evidence of an interfering species in the O_3 and NO_2 measurements, although substantially smaller (Figures S14, S18, and S19). Similar to the 27 June Thanksgiving experiment, the base model underestimated the OH measurements from this day by an average of 62% in the afternoon and evening. However, unlike the Thanksgiving experiment, there was not a clear, consistent interference in the O_3 measurements to scale the concentration of the photolytic VOC interference in the model. Assuming that the interference was emitted by the gas stove, the average ratio of the concentration of the photolytic interference to the NO_2 concentration measured by the CAPS instrument during cooking and noncooking periods was calculated for the model run that best fit the Thanksgiving data. The concentration of additional photolytic VOC input into the model for the 12 June experiment was then calculated based on this ratio, resulting in a maximum of about 2.7 ppb (Figure S16). Because of the estimation required to calculate the concentration of the photolytic VOC, the model was run with a VOC concentration of ±50%, with the results indicated by the shaded region. As with the Thanksgiving experiment, the addition of the photolytic VOC improves the overall agreement between the model and the measured values (Figure 5), with a median measured/model ratio of 1.08 (quartiles = 0.35, 1.8) compared to 2.1 (quartiles = 1.2, 4.5) for the base case. However, the measured maximum concentration is approximately 1 h later than predicted by the model, occurring after peak concentrations of compounds emitted by the gas stove and the maximum sunlight intensity. While the true cause of this discrepancy is unclear, one explanation is that similar to the Thanksgiving experiment, the presence of people in the house created a localized sink during the peak OH concentrations. Although the concentration of the photolytic VOC is lower compared to the Thanksgiving experiment, the model is able to reproduce the high concentrations of OH observed on this day as the lower mixing ratios of NO_2 result in lower rates of OH radical termination.

The modeled HO_2 is also in better agreement with the measured HO_2* during the early evening (17:00−19:00). The measured peak during a ventilation period is likely at least partially due to the infiltration of outdoor HO_2, which is not included in the model. However, elevated model concentrations occur as the concentration of NO and NO_2 decrease during the ventilation period, reducing radical sinks and elevating the steady-state concentration of HO_2.

https://doi.org/10.1021/acs.est.2c05756
Environ. Sci. Technol. 2023, 57, 896−908

3.7. Environmental Implications. An unknown photolytic radical source tied to the use of cooking with gas appliances can significantly alter the oxidative capacity of indoor environments. Adding this radical source into the chemical model greatly improves the agreement with measured concentrations of OH radicals, both during normal use of the gas stove and the more extreme case of cooking a large Thanksgiving meal for multiple hours. In the model, the novel source was primarily responsible for the production of radicals, and while the model used estimates and assumptions for the concentration, photolysis frequency, and reaction pathway of the unknown radical source, a compound with lower concentrations and a higher photolysis frequency could produce similar results, and vice versa. However, to explain the discrepancy in the O_3 and NO_2 instruments, concentrations of the interference would need to be higher than measurements of any other potential interfering compounds. During HOMEChem, there was no evidence of a photolabile interference in either the NO_2 or O_3 instruments outside of cooking experiments. While this radical source can alter the oxidative capacity during gas cooking, there is no evidence that it is a common compound in indoor air.

Studies on indoor photolysis have primarily focused on the photolysis of small molecules such as HCHO, HONO, HOCl, and Cl_2.[12,13,60] Indoor environments can have higher concentrations of several oxygenated and otherwise functionalized VOCs which can photolyze to form radicals and may be overlooked in current indoor chemical mechanisms.[61,62] Cooking, and even just the heating of oil, can produce a large variety of functionalized VOCs that can further react or photolyze to influence the indoor environment. While many compounds were measured at HOMEChem,[29,62] highly functionalized molecules may be difficult to measure if they are lost in long sampling lines or fragments within instrumentation. If these compounds remain unmeasured and uncharacterized, our understanding of indoor oxidative capacity during cooking events is severely limited. The presence of additional radical sources would increase overall VOC oxidation, resulting in increased production of secondary organic aerosols and other potentially harmful compounds, such as aldehydes, ketones, acids, and peroxides.[63−65] To our knowledge, these results are the first direct measurements of OH in a residential setting, indicating that significant OH concentrations can occur in houses during normal occupancy behavior, enhancing the oxidative capacity and the potential for chemical transformations and aerosol formation in the indoor environment.

■ ASSOCIATED CONTENT

Supporting Information

The Supporting Information is available free of charge at https://pubs.acs.org/doi/10.1021/acs.est.2c05756.

Photostationary state calculation of ozone concentrations; discussion of the discrepancy between O_3 instruments; estimation of interference photolysis rates; and radical budget analysis, Tables S1 and S2, Figures S1−S21 (PDF)

■ AUTHOR INFORMATION

Corresponding Authors

Emily Reidy − *Department of Chemistry, Indiana University, Bloomington, Indiana 47405, United States*; Email: ekreidy@indiana.edu

Philip S. Stevens − *Department of Chemistry and O'Neill School of Public and Environmental Affairs, Indiana University, Bloomington, Indiana 47405, United States*; orcid.org/0000-0001-9899-4215; Email: pstevens@indiana.edu

Authors

Brandon P. Bottorff − *Department of Chemistry, Indiana University, Bloomington, Indiana 47405, United States*; Present Address: O'Neill School of Public and Environmental Affairs, Indiana University, Bloomington, Indiana 47405, United States; orcid.org/0000-0002-5145-0031

Colleen Marciel F. Rosales − *O'Neill School of Public and Environmental Affairs, Indiana University, Bloomington, Indiana 47405, United States*; Present Address: Air Quality Research Center, University of California, Davis, California 95616, United States.; Present Address: OpenAQ, Washington, DC 20016, United States.; orcid.org/0000-0002-8925-8352

Felipe J. Cardoso-Saldaña − *McKetta Department of Chemical Engineering, University of Texas, Austin, Texas 78712, United States*; Present Address: Exxon-Mobil Upstream Research Company, Spring, Texas 77389, United States.; orcid.org/0000-0002-6359-8076

Caleb Arata − *Department of Environmental Science, Policy, and Management, University of California, Berkeley, California 94720, United States*

Shan Zhou − *Department of Chemistry, Syracuse University, Syracuse, New York 13244, United States*; Present Address: Department of Earth and Atmospheric Sciences, University of Houston, Houston, Texas 77004, United States.; orcid.org/0000-0001-5031-1024

Chen Wang − *Department of Chemistry, University of Toronto, Toronto, Ontario M5S 3H6, Canada*; Present Address: School of Environmental Science and Engineering, Southern University of Science and Technology, Shenzhen 518055, China; orcid.org/0000-0001-9565-8777

Andrew Abeleira − *Department of Chemistry, Colorado State University, Fort Collins, Colorado 80523, United States*

Lea Hildebrandt Ruiz − *McKetta Department of Chemical Engineering, University of Texas, Austin, Texas 78712, United States*; orcid.org/0000-0001-8378-1882

Allen H. Goldstein − *Department of Environmental Science, Policy, and Management, University of California, Berkeley, California 94720, United States*; orcid.org/0000-0003-4014-4896

Atila Novoselac − *Department of Civil, Architectural, and Environmental Engineering, University of Texas, Austin, Texas 78712, United States*

Tara F. Kahan − *Department of Chemistry, Syracuse University, Syracuse, New York 13244, United States; Department of Chemistry, University of Saskatchewan, Saskatoon, Saskatchewan S7N 5E6, Canada*; orcid.org/0000-0001-5074-1155

https://doi.org/10.1021/acs.est.2c05756
Environ. Sci. Technol. 2023, 57, 896−908

Jonathan P. D. Abbatt − *Department of Chemistry, University of Toronto, Toronto, Ontario M5S 3H6, Canada;* orcid.org/0000-0002-3372-334X

Marina E. Vance − *Department of Mechanical Engineering, University of Colorado, Boulder, Colorado 80309, United States;* orcid.org/0000-0003-0940-0353

Delphine K. Farmer − *Department of Chemistry, Colorado State University, Fort Collins, Colorado 80523, United States;* orcid.org/0000-0002-6470-9970

Complete contact information is available at: https://pubs.acs.org/10.1021/acs.est.2c05756

Notes

The authors declare no competing financial interest.

■ ACKNOWLEDGMENTS

We would like to thank the Alfred P. Sloan Foundation for funding the HOMEChem campaign and analysis (G-2017-9944 and G-2018-11061), as well as all members of the HOMEChem Science Team.

■ REFERENCES

(1) Griffith, S. M.; Hansen, R.; Dusanter, S.; Michoud, V.; Gilman, J.; Kuster, W.; Veres, P.; Graus, M.; de Gouw, J.; Roberts, J.; Young, C.; Washenfelder, R.; Brown, S. S.; Thalman, R.; Waxman, E.; Volkamer, R.; Tsai, C.; Stutz, J.; Flynn, J. H.; Grossberg, N.; Lefer, B.; Alvarez, S. L.; Rappenglueck, B.; Mielke, L. H.; Osthoff, H. D.; Stevens, P. S. Measurements of hydroxyl and hydroperoxy radicals during CalNex-LA: Model comparisons and radical budgets. *J. Geophys. Res. D: Atmos.* **2016**, *121*, 4211−4232.

(2) Ren, X.; Harder, H.; Martinez, M.; Lesher, R. L.; Oliger, A.; Simpas, J. B.; Brune, W. H.; Schwab, J. J.; Demerjian, K. L.; He, Y. OH and HO2 chemistry in the urban atmosphere of New York City. *Atmos. Environ.* **2003**, *37*, 3639−3651.

(3) Zhang, G.; Hu, R.; Xie, P.; Lou, S.; Wang, F.; Wang, Y.; Qin, M.; Li, X.; Liu, X.; Wang, Y.; Liu, W. Observation and simulation of HOx radicals in an urban area in Shanghai, China. *Sci. Total Environ.* **2022**, *810*, No. 152275.

(4) Sommariva, R.; Crilley, L. R.; Ball, S. M.; Cordell, R. L.; Hollis, L. D.; Bloss, W. J.; Monks, P. S. Enhanced wintertime oxidation of VOCs via sustained radical sources in the urban atmosphere. *Environ. Pollut.* **2021**, *274*, No. 116563.

(5) Xue, L.; Gu, R.; Wang, T.; Wang, X.; Saunders, S.; Blake, D.; Louie, P. K.; Luk, C. W.; Simpson, I.; Xu, Z.; Wang, Z.; Gao, Y.; Lee, S.; Mellouki, A.; Wang, W. Oxidative capacity and radical chemistry in the polluted atmosphere of Hong Kong and Pearl River Delta region: analysis of a severe photochemical smog episode. *Atmos. Chem. Phys.* **2016**, *16*, 9891−9903.

(6) Alicke, B.; Geyer, A.; Hofzumahaus, A.; Holland, F.; Konrad, S.; Pätz, H. W.; Schäfer, J.; Stutz, J.; Volz-Thomas, A.; Platt, U. OH formation by HONO photolysis during the BERLIOZ experiment. *J. Geophys. Res.: Atmos.* **2003**, *108*, PHO 3-1−PHO 3-17.

(7) Aumont, B.; Chervier, F.; Laval, S. Contribution of HONO sources to the NOx/HOx/O3 chemistry in the polluted boundary layer. *Atmos. Environ.* **2003**, *37*, 487−498.

(8) Sörgel, M.; Regelin, E.; Bozem, H.; Diesch, J.-M.; Drewnick, F.; Fischer, H.; Harder, H.; Held, A.; Hosaynali-Beygi, Z.; Martinez, M.; Zetzsch, C. Quantification of the unknown HONO daytime source and its relation to NO 2. *Atmos. Chem. Phys.* **2011**, *11*, 10433−10447.

(9) Elshorbany, Y. F.; Kleffmann, J.; Kurtenbach, R.; Lissi, E.; Rubio, M.; Villena, G.; Gramsch, E.; Rickard, A.; Pilling, M.; Wiesen, P. Seasonal dependence of the oxidation capacity of the city of Santiago de Chile. *Atmos. Environ.* **2010**, *44*, 5383−5394.

(10) Griffith, S.; Hansen, R.; Dusanter, S.; Stevens, P.; Alaghmand, M.; Bertman, S.; Carroll, M.; Erickson, M.; Galloway, M.; Grossberg, N.; Hottle, J.; Hou, J.; Jobson, B. T.; Kammrath, A.; Keutsch, F. N.; Lefer, B. L.; Mielke, L. H.; O'Brien, A.; Shepson, P. B.; Thurlow, M.; Wallace, W.; Zhang, N.; Zhou, X. L. OH and HO 2 radical chemistry during PROPHET 2008 and CABINEX 2009−Part 1: Measurements and model comparison. *Atmos. Chem. Phys.* **2013**, *13*, 5403−5423.

(11) Mao, J.; Ren, X.; Zhang, L.; Van Duin, D.; Cohen, R.; Park, J.-H.; Goldstein, A.; Paulot, F.; Beaver, M.; Crounse, J. Insights into hydroxyl measurements and atmospheric oxidation in a California forest. *Atmos. Chem. Phys.* **2012**, *12*, 8009−8020.

(12) Kowal, S. F.; Allen, S. R.; Kahan, T. F. Wavelength-resolved photon fluxes of indoor light sources: Implications for HO x production. *Environ. Sci. Technol.* **2017**, *51*, 10423−10430.

(13) Zhou, S.; Kowal, S. F.; Cregan, A. R.; Kahan, T. F. Factors affecting wavelength-resolved ultraviolet irradiance indoors and their impacts on indoor photochemistry. *Indoor Air* **2021**, *31*, 1187−1198.

(14) Gandolfo, A.; Gligorovski, V.; Bartolomei, V.; Tlili, S.; Gómez Alvarez, E.; Wortham, H.; Kleffmann, J.; Gligorovski, S. Spectrally resolved actinic flux and photolysis frequencies of key species within an indoor environment. *Build. Environ.* **2016**, *109*, 50−57.

(15) Gligorovski, S. Nitrous acid (HONO): An emerging indoor pollutant. *J. Photochem. Photobiol., A* **2016**, *314*, 1−5.

(16) Traynor, G. W.; Anthon, D. W.; Hollowell, C. D. Technique for determining pollutant emissions from a gas-fired range. *Atmos. Environ.* **1982**, *16*, 2979−2987.

(17) Singer, B. C.; Pass, R. Z.; Delp, W. W.; Lorenzetti, D. M.; Maddalena, R. L. Pollutant concentrations and emission rates from natural gas cooking burners without and with range hood exhaust in nine California homes. *Build. Environ.* **2017**, *122*, 215−229.

(18) Zhou, S.; Young, C. J.; VandenBoer, T. C.; Kowal, S. F.; Kahan, T. F. Time-resolved measurements of nitric oxide, nitrogen dioxide, and nitrous acid in an occupied New York home. *Environ. Sci. Technol.* **2018**, *52*, 8355−8364.

(19) Liu, J.; Li, S.; Zeng, J.; Mekic, M.; Yu, Z.; Zhou, W.; Loisel, G.; Gandolfo, A.; Song, W.; Wang, X.; Zhou, Z.; Herrmann, H.; Li, X.; Gligorovski, S. Assessing indoor gas phase oxidation capacity through real-time measurements of HONO and NOx in Guangzhou, China. *Environ. Sci. Processes Impacts* **2019**, *21*, 1393−1402.

(20) Finlayson-Pitts, B. J.; Pitts, J. N., Jr.*Chemistry of the upper and lower atmosphere: theory, experiments, and applications*; Elsevier, 1999.

(21) Hallquist, M.; Wenger, J. C.; Baltensperger, U.; Rudich, Y.; Simpson, D.; Claeys, M.; Dommen, J.; Donahue, N.; George, C.; Goldstein, A.; Hamilton, J. F.; Herrmann, H.; Hoffmann, T.; Iinuma, Y.; Jang, M.; Jenkin, M. E.; Jimenez, J. L.; Kiendler-Scharr, A.; Maenhaut, W.; McFiggans, G.; Mentel, T. F.; Monod, A.; Prévôt, A. S. H.; Seinfeld, J. H.; Surratt, J. D.; Szmigielski, R.; Wildt, J. The formation, properties and impact of secondary organic aerosol: current and emerging issues. *Atmos. Chem. Phys.* **2009**, *9*, 5155−5236.

(22) Mauderly, J. L.; Chow, J. C. Health effects of organic aerosols. *Inhalation Toxicol.* **2008**, *20*, 257−288.

(23) Gomez Alvarez, E.; Amedro, D.; Afif, C.; Gligorovski, S.; Schoemaecker, C.; Fittschen, C.; Doussin, J.-F.; Wortham, H. Unexpectedly high indoor hydroxyl radical concentrations associated with nitrous acid. *Proc. Natl. Acad. Sci. U. S. A.* **2013**, *110*, 13294−13299.

(24) Mendez, M.; Amedro, D.; Blond, N.; Hauglustaine, D. A.; Blondeau, P.; Afif, C.; Fittschen, C.; Schoemaecker, C. Identification of the major HOx radical pathways in an indoor air environment. *Indoor Air* **2017**, *27*, 434−442.

(25) Heard, D. E.; Pilling, M. J. Measurement of OH and HO2 in the troposphere. *Chem. Rev.* **2003**, *103*, 5163−5198.

(26) Carslaw, N.; Fletcher, L.; Heard, D.; Ingham, T.; Walker, H. Significant OH production under surface cleaning and air cleaning conditions: Impact on indoor air quality. *Indoor Air* **2017**, *27*, 1091−1100.

(27) Fiorentino, E.-A.; Chen, H.; Gandolfo, A.; Lannuque, V.; Sartelet, K.; Wortham, H. Measurements and Modelling of OH and Peroxy Radicals in an Indoor Environment Under Different Light Conditions and VOC Levels. *Atmos. Environ.* **2023**, *292*, No. 119398.

(28) Lakey, P. S. J.; Won, Y.; Shaw, D.; Østerstrøm, F. F.; Mattila, J.; Reidy, E.; Bottorff, B.; Rosales, C.; Wang, C.; Ampollini, L.; et al.

Spatial and temporal scales of variability for indoor air constituents. *Commun. Chem.* **2021**, *4*, 110.
(29) Farmer, D. K.; Vance, M. E.; Abbatt, J. P.; Abeleira, A.; Alves, M. R.; Arata, C.; Boedicker, E.; Bourne, S.; Cardoso-Saldaña, F.; Corsi, R.; DeCarlo, P. F.; Goldstein, A. H.; Grassian, V. H.; Hildebrandt Ruiz, L.; Jimenez, J. L.; Kahan, T. F.; Katz, E. F.; Mattila, J. M.; Nazaroff, W. W.; Novoselac, A.; O'Brien, R. E.; Or, V. W.; Patel, S.; Sankhyan, S.; Stevens, P. S.; Tian, Y.; Wade, M.; Wang, C.; Zhou, S.; Zhou, Y. Overview of HOMEChem: House observations of microbial and environmental chemistry. *Environ. Sci. Processes Impacts* **2019**, *21*, 1280−1300.
(30) Abeleira, A.; Pollack, I. B.; Sive, B.; Zhou, Y.; Fischer, E. V.; Farmer, D. K. Source characterization of volatile organic compounds in the Colorado Northern Front Range Metropolitan Area during spring and summer 2015. *J. Geophys. Res.: Atmos.* **2017**, *122*, 3595−3613.
(31) Zhou, S.; Kahan, T. F. Spatiotemporal characterization of irradiance and photolysis rate constants of indoor gas-phase species in the UTest house during HOMEChem. *Indoor Air* **2022**, *32*, No. e12964.
(32) Wang, C.; Bottorff, B.; Reidy, E.; Rosales, C. M. F.; Collins, D. B.; Novoselac, A.; Farmer, D. K.; Vance, M. E.; Stevens, P. S.; Abbatt, J. P. Cooking, bleach cleaning, and air conditioning strongly impact levels of HONO in a house. *Environ. Sci. Technol.* **2020**, *54*, 13488−13497.
(33) Bottorff, B.; Reidy, E.; Mielke, L.; Dusanter, S.; Stevens, P. S. Development of a laser-photofragmentation laser-induced fluorescence instrument for the detection of nitrous acid and hydroxyl radicals in the atmosphere. *Atmos. Meas. Tech.* **2021**, *14*, 6039−6056.
(34) Lew, M. M.; Dusanter, S.; Stevens, P. S. Measurement of interferences associated with the detection of the hydroperoxy radical in the atmosphere using laser-induced fluorescence. *Atmos. Meas. Tech.* **2018**, *11*, 95−109.
(35) Dusanter, S.; Vimal, D.; Stevens, P. Measuring tropospheric OH and HO 2 by laser-induced fluorescence at low pressure. A comparison of calibration techniques. *Atmos. Chem. Phys.* **2008**, *8*, 321−340.
(36) Goliff, W. S.; Stockwell, W. R.; Lawson, C. V. The regional atmospheric chemistry mechanism, version 2. *Atmos. Environ.* **2013**, *68*, 174−185.
(37) Wolfe, G. M.; Marvin, M. R.; Roberts, S. J.; Travis, K. R.; Liao, J. The framework for 0-D atmospheric modeling (F0AM) v3.1. *Geosci. Model Dev.* **2016**, *9*, 3309−3319.
(38) Cotte, H.; Devaux, C.; Carlier, P. Transformation of irradiance measurements into spectral actinic flux for photolysis rates determination. *J. Atmos. Chem.* **1997**, *26*, 1−28.
(39) Spicer, C. W.; Kenny, D. V.; Ward, G. F.; Billick, I. H. Transformations, lifetimes, and sources of NO2, HONO, and HNO3 in indoor environments. *J. Air Waste Manage. Assoc.* **1993**, *43*, 1479−1485.
(40) Weschler, C. J.; Carslaw, N. Indoor chemistry. *Environ. Sci. Technol.* **2018**, *52*, 2419−2428.
(41) Zannoni, N.; Lakey, P. S.; Won, Y.; Shiraiwa, M.; Rim, D.; Weschler, C. J.; Wang, N.; Ernle, L.; Li, M.; Bekö, G.; Wargocki, P.; Williams, J. The human oxidation field. *Science* **2022**, *377*, 1071−1077.
(42) Wang, W.; Yuan, B.; Peng, Y.; Su, H.; Cheng, Y.; Yang, S.; Wu, C.; Qi, J.; Bao, F.; Huangfu, Y.; et al. Direct observations indicate photodegradable oxygenated volatile organic compounds (OVOCs) as larger contributors to radicals and ozone production in the atmosphere. *Atmos. Chem. Phys.* **2022**, *22*, 4117−4128.
(43) Krapf, M.; El Haddad, I.; Bruns, E. A.; Molteni, U.; Daellenbach, K. R.; Prévôt, A. S.; Baltensperger, U.; Dommen, J. Labile peroxides in secondary organic aerosol. *Chem* **2016**, *1*, 603−616.
(44) Badali, K. M.; Zhou, S.; Aljawhary, D.; Antiñolo, M.; Chen, W. J.; Lok, A.; Mungall, E.; Wong, J. P. S.; Zhao, R.; Abbatt, J. P. D. Formation of hydroxyl radicals from photolysis of secondary organic aerosol material. *Atmos. Chem. Phys.* **2015**, *15*, 7831−7840.
(45) Rickly, P.; Stevens, P. S. Measurements of a potential interference with laser-induced fluorescence measurements of ambient OH from the ozonolysis of biogenic alkenes. *Atmos. Meas. Tech.* **2018**, *11*, 1−16.
(46) Davis, D.; Rodgers, M.; Fischer, S.; Asai, K. An experimental assessment of the O3/H2O interference problem in the detection of natural levels of OH via laser induced fluorescence. *Geophys. Res. Lett.* **1981**, *8*, 69−72.
(47) Davis, D.; Rodgers, M.; Fischer, S.; Heaps, W. A theoretical assessment of the O3/H2O interference problem in the detection of natural levels of OH via laser induced fluorescence. *Geophys. Res. Lett.* **1981**, *8*, 73−76.
(48) Fittschen, C.; Al Ajami, M.; Batut, S.; Ferracci, V.; Archer-Nicholls, S.; Archibald, A. T.; Schoemaecker, C. ROOOH: a missing piece of the puzzle for OH measurements in low-NO environments? *Atmos. Chem. Phys.* **2019**, *19*, 349−362.
(49) Schwartz-Narbonne, H.; Abbatt, J. P.; DeCarlo, P. F.; Farmer, D. K.; Mattila, J. M.; Wang, C.; Donaldson, D. J.; Siegel, J. A. Modeling the Removal of Water-Soluble Trace Gases from Indoor Air via Air Conditioner Condensate. *Environ. Sci. Technol.* **2021**, *55*, 10987−10993.
(50) Turnipseed, A. A.; Andersen, P. C.; Williford, C. J.; Ennis, C. A.; Birks, J. W. Use of a heated graphite scrubber as a means of reducing interferences in UV-absorbance measurements of atmospheric ozone. *Atmos. Meas. Tech.* **2017**, *10*, 2253−2269.
(51) Spicer, C. W.; Joseph, D. W.; Ollison, W. M. A re-examination of ambient air ozone monitor interferences. *J. Air Waste Manage. Assoc.* **2010**, *60*, 1353−1364.
(52) Kenner, R.; Rohrer, F.; Stuhl, F. Hydroxyl (A) production in the 193-nm photolysis of nitrous acid. *J. Phys. Chem.* **1986**, *90*, 2635−2639.
(53) Martinez, R. D.; Buitrago, A. A.; Howell, N. W.; Hearn, C. H.; Joens, J. A. The near UV absorption spectra of several aliphatic aldehydes and ketones at 300 K. *Atmos. Environ. A* **1992**, *26*, 785−792.
(54) Keller-Rudek, H.; Moortgat, G. K.; Sander, R.; Sörensen, R. The MPI-Mainz UV/VIS Spectral Atlas of Gaseous Molecules of Atmospheric Interest. *Earth Syst. Sci. Data* **2013**, *5*, 365−373.
(55) Villena, G.; Bejan, I.; Kurtenbach, R.; Wiesen, P.; Kleffmann, J. Interferences of commercial NO 2 instruments in the urban atmosphere and in a smog chamber. *Atmos. Meas. Tech.* **2012**, *5*, 149−159.
(56) Pereira Da Costa, M.; Conte-Junior, C. A. Chromatographic methods for the determination of carbohydrates and organic acids in foods of animal origin. *Compr. Rev. Food Sci. Food Saf.* **2015**, *14*, 586−600.
(57) Klampfl, C. W. Determination of organic acids by CE and CEC methods. *Electrophoresis* **2007**, *28*, 3362−3378.
(58) Lopez-Hilfiker, F. D.; Iyer, S.; Mohr, C.; Lee, B. H.; D'Ambro, E. L.; Kurtén, T.; Thornton, J. A. Constraining the sensitivity of iodide adduct chemical ionization mass spectrometry to multifunctional organic molecules using the collision limit and thermodynamic stability of iodide ion adducts. *Atmos. Meas. Tech.* **2016**, *9*, 1505−1512.
(59) Mattila, J. M.; Lakey, P. S.; Shiraiwa, M.; Wang, C.; Abbatt, J. P.; Arata, C.; Goldstein, A. H.; Ampollini, L.; Katz, E. F.; DeCarlo, P. F.; Zhou, S.; Kahan, T. F.; Cardoso-Saldaña, F. J.; Ruiz, L. H.; Abeleira, A.; Boedicker, E. K.; Vance, M. E.; Farmer, D. K. Multiphase chemistry controls inorganic chlorinated and nitrogenated compounds in indoor air during bleach cleaning. *Environ. Sci. Technol.* **2020**, *54*, 1730−1739.
(60) Wang, Z.; Kowal, S. F.; Carslaw, N.; Kahan, T. F. Photolysis-driven indoor air chemistry following cleaning of hospital wards. *Indoor Air* **2020**, *30*, 1241−1255.
(61) Takhar, M.; Li, Y.; Ditto, J. C.; Chan, A. W. Formation pathways of aldehydes from heated cooking oils. *Environ. Sci. Processes Impacts* **2022**, DOI: 10.1039/D1EM00532D.
(62) Arata, C.; Misztal, P. K.; Tian, Y.; Lunderberg, D. M.; Kristensen, K.; Novoselac, A.; Vance, M. E.; Farmer, D. K.; Nazaroff,

W. W.; Goldstein, A. H. Volatile organic compound emissions during HOMEChem. *Indoor Air* **2021**, *31*, 2099−2117.
(63) Hakola, H.; Arey, J.; Aschmann, S. M.; Atkinson, R. Product formation from the gas-phase reactions of OH radicals and O3 with a series of monoterpenes. *J. Atmos. Chem.* **1994**, *18*, 75−102.
(64) Lee, A.; Goldstein, A. H.; Kroll, J. H.; Ng, N. L.; Varutbangkul, V.; Flagan, R. C.; Seinfeld, J. H. Gas-phase products and secondary aerosol yields from the photooxidation of 16 different terpenes. *J. Geophys. Res.: Atmos.* **2006**, 111.
(65) Jones, A. P. Indoor air quality and health. *Atmos. Environ.* **1999**, *33*, 4535−4564.

https://doi.org/10.1021/acs.est.2c05756
Environ. Sci. Technol. 2023, 57, 896−908